Protective human monoclonal antibodies that target the Type III Secretion System of *Pseudomonas aeruginosa* inhibit translocon function

Jean-Mathieu Desveaux[1], Eric Faudry[1], Carlos Contreras-Martel[1], François Cretin[1], Leonardo Sebastian Dergan-Dylon[1], Axelle Amen[1,2], Isabelle Bally[1], Victor Tardivy-Casemajor[1], Fabien Chenavier[1], Delphine Fouquenet[3], Yvan Caspar[1,4], Ina Attrée*[1], Andréa Dessen*[1], Pascal Poignard*[1]

[1] Univ. Grenoble Alpes, CEA, CNRS, Institut de Biologie Structurale (IBS), F-38044 Grenoble, France

[2] Laboratoire d'Immunologie, CHU Grenoble Alpes, France

[3]Centre d'Étude des Pathologies Respiratoires INSERM U1100 UFR de Médecine de Tours, 10 Bd Tonnellé, 37032 Tours Cedex

[4] Laboratoire de Bactériologie-Hygiène Hospitalière, CHU Grenoble Alpes, France

* to whom correspondence should be addressed: ina.attree@ibs.fr, andrea.dessen@ibs.fr, pascal.poignard@ibs.fr

ABSTRACT

Pseudomonas aeruginosa is a major human opportunistic pathogen associated with a high incidence of multi-drug resistance. The antibody-based blockade of *P. aeruginosa* virulence factors represents a promising alternative strategy to mitigate its infectivity. In this study, we employed single B cell sorting to isolate, from cystic fibrosis patients, human monoclonal antibodies (mAbs) targeting proteins from the *P. aeruginosa* Type 3 Secretion System (T3SS) and characterized a panel of mAbs directed at PscF and PcrV. Among those, two mAbs, P5B3 and P3D6, that bind to the injectisome tip protein PcrV, exhibited T3SS blocking activity. We solved the crystal structure of the P3D6 Fab-PcrV complex, which revealed that the Ab binds to the C-terminal region of PcrV. Further, we compared the T3SS-blocking activity of three PcrV-targeting mAbs, including two from previous independent studies, using two distinct assays to evaluate pore formation and toxin injection. We conducted a mechanistic and structural analysis of their modes of action through modeling based on the known structure of a functional homolog, SipD from *Salmonella typhimurium*. The analysis suggests that anti-PcrV mAbs may act through different mechanisms, ranging from preventing PcrV oligomerization to disrupting PcrV's scaffolding function, thereby inhibiting the assembly and function of the translocon pore. Our findings provide additional evidence that T3SS-targeting Abs, some capable of inhibiting virulence, are elicited in *P. aeruginosa*-infected patients. The results offer deeper insights into PcrV recognition by mAbs and their associated mechanisms of action, helping to identify which Abs are more likely to be therapeutically useful based on their mode of action and potency. This paves the way for developing effective alternatives to traditional antibiotics in the fight against this resilient pathogen.

INTRODUCTION

The emergence of antimicrobial resistance is a major threat to human health. Among the microorganisms whose resistance rates have increased the most dramatically are ESKAPE pathogens (***E****nterococcus faecium,* ***S****taphylococcus aureus,* ***K****lebsiella pneumoniae,* ***A****cinetobacter baumannii,* ***P****seudomonas aeruginosa,* ***E****nterobacter spp*) for which novel antibacterial treatments are urgently needed. However, an antibiotic discovery hiatus that occurred during the last few decades severely heightened the resistance threat (Murray et al., 2022), underlining the importance of exploring alternative strategies such as host-targeting, bacteriophage, anti-virulence, and Ab-based therapies (De Melo et al., 2024; Kaufmann et al., 2018; Morrison, 2015).

Therapeutic mAbs have been successfully developed to fight viral infections ranging from Ebola to SARS-CoV-2 (Crowe, 2022; Levin et al., 2022; Mulangu et al., 2019). To date, however, only three therapeutic Abs have been marketed against bacteria, all of which target toxins. Other types of bacterial virulence factors could also serve as potential high importance targets for mAbs. Recent examples include the development of mAbs that target lipopolysaccharides, O-antigen, and outer membrane transporter proteins, notably in *Klebsiella pneumoniae* and *Mycobacterium tuberculosis* (Pennini et al., 2017; Rollenske et al., 2018; Watson et al., 2021). The advantages of targeting virulence factors through mAbs include notably a high specificity and the decreased likelihood of the emergence of resistance among bacteria (La Guidara et al., 2024). Additionally, the employment of mAb engineering platforms offers the potential for improved efficacy through modifications such as half-life extension and alterations of Fc effector functions (Morrison, 2015; Vacca et al., 2022). Finally, strategies such as the use of mAb cocktails targeting different specificities and the combination with traditional antibiotics further expand the range of Ab-based treatment options (Duan et al., 2021; Morrison, 2015; Tabor et al., 2018).

Pseudomonas aeruginosa is a major nosocomial pathogen and the leading cause of acute pneumonia and chronic lung infections, particularly in ventilator-assisted and cystic fibrosis (CF) patients. Infections with *P. aeruginosa* ultimately lead to loss of lung function and death in CF patients. Worldwide, *P. aeruginosa* is responsible for more than 300,000 deaths associated or attributed to resistance each year. The natural resistance of *P. aeruginosa* to a broad range of antibiotics, its ability

88 to grow as biofilms, as well as its widespread presence in hospital settings (Horcajada
89 et al., 2019; Murray et al., 2022), have called for urgent efforts towards the
90 development of new therapeutic agents. Aggressive acute infections by *P. aeruginosa*
91 are highly dependent on its Type III Secretion System (T3SS), a needle-like, multi-
92 component secretion machinery located on the cell surface and that transports
93 effectors from the bacterial cytoplasm directly into the host cell cytosol (Goure et al.,
94 2004; Hauser, 2009; Quinaud et al., 2007, 2005). It is of note that in other human
95 pathogens such as *Yersinia pestis*, *Salmonella typhi*, *Shigella dysenteriae* and
96 *Escherichia coli* the T3SS also plays a key role in virulence, participating in the
97 causation of diseases such as plague, typhoid fever, and bacillary dysentery,
98 respectively (Coburn et al., 2007; Diepold and Wagner, 2014; Hu et al., 2017; Serapio-
99 Palacios and Finlay, 2020).

100 A key component of the T3SS is the injectisome, membrane-embedded protein
101 rings extended by a hollow needle, composed of the PscF protein that protrudes
102 outwards from the bacterial surface. Injectisome-dependent toxin delivery, which
103 occurs upon contact with the eukaryotic target cell, also requires formation of the
104 'translocon', a complex of three proteins that are exported through the interior of the
105 polymerized needle, assemble at its tip and form a pore in the eukaryotic cell
106 membrane, an essential step for effector injection (Mueller et al., 2008). The translocon
107 is composed of two hydrophobic proteins (PopB and PopD in *P. aeruginosa*), as well
108 as a hydrophilic partner - PcrV, or the V antigen- in *P. aeruginosa* (Matteï et al., 2011).
109 PopB and PopD have been shown to act as *bona fide* pore-forming toxins (Schoehn
110 et al., 2003; Faudry et al., 2006; Montagner et al., 2011) that, upon membrane
111 disruption, can trigger the manipulation of host processes including histone
112 dephosphorylation and mitochondrial network disruption (Dortet et al., 2018). PcrV, on
113 the other hand, oligomerizes at the tip of the T3SS needle and aids PopB and PopD in
114 their membrane disruption process (Gébus et al., 2009; Goure et al., 2005; Guo and
115 Galán, 2021; Matteï et al., 2011). Crystal structures of monomeric homologs of PcrV
116 (LcrV, SipD, BipD) have shown that they fold into an elongated coiled-coil buttressed
117 by an α-helical hairpin at the N-terminus and an α/β carboxy-terminal region
118 (Derewenda, 2011; Erskine et al., 2006; Lunelli et al., 2011). Notably, the cryo-EM
119 structure of a needle filament complex composed of PrgI (needle protein) with SipD
120 (tip protein) at its extremity confirmed that the latter forms a pentamer where the first

121 and fifth subunits are separated by a gap, thus generating a heterogeneous assembly
122 (Guo and Galán, 2021). This arrangement could be similar in numerous T3SS systems
123 (Habenstein et al., 2019).

124 Given the importance of the T3SS for *P. aeruginosa* infection, components such
125 as PcrV and PscF have been explored as targets for the development of therapeutic
126 Abs and inhibitory small molecules, respectively (Berube et al., 2017; Bowlin et al.,
127 2014). Animal models have shown that blocking the T3SS, particularly the function of
128 PcrV, can successfully diminish tissue damage due to *P. aeruginosa* infection (Frank
129 et al., 2002; Imamura et al., 2007). Moreover, in ventilated patients, pegylated Fabs
130 that target PcrV (KB001-A) were shown to successfully reduce the incidence of
131 pneumonia, which is consistent with the role of T3SS in the acute phase of infection
132 (Jain et al., 2018; Roy-Burman et al., 2001). However, this treatment did not benefit
133 chronically colonized CF patients in terms of antibiotic needs (François et al., 2012;
134 Jain et al., 2018; Yaeger et al., 2021). In addition, the bispecific MEDI3902 mAb
135 targeting both PcrV and the Psl exopolysaccharide successfully protected against *P.*
136 *aeruginosa* infection in animal models but was discontinued in phase II clinical trials
137 (Chastre et al., 2022; DiGiandomenico et al., 2014). Nevertheless, PcrV remains an
138 attractive target, motivating the search for potentially more effective Abs (Simonis et
139 al., 2023).

140 Here, we sorted specific single memory B cells from peripheral blood
141 mononuclear cells (PBMCs) of cystic fibrosis patients to identify mAbs against PcrV
142 and PscF with potential T3SS-inhibiting activity. Two anti-PcrV mAbs (P5B3 and P3D6)
143 showed inhibition of the injection of the T3SS effector ExoS into epithelial cells, with
144 mAb P5B3 displaying blocking activity against five major PcrV variants representing
145 more than 80% of clinical isolates sequenced to date. We obtained the crystal structure
146 of a P3D6 Fab-PcrV complex and further compared the mechanisms of actions of
147 different anti-PcrV mAbs targeting various epitopes, including one mAb from a recent
148 publication (Simonis et al., 2023). These structure-based analyses of the mechanisms
149 of action of the different mAbs provide valuable insights for the development of
150 improved antipseudomonal treatments and preventive approaches.

151

152

153 **RESULTS**

154

155 **Selection of donors exhibiting T3SS-inhibiting circulating IgG responses**

156 Our approach was based on single cell sorting of recombinant PcrV and PscF
157 specific memory B cells from human donor peripheral blood mononuclear cells
158 (PBMCs). To identify donors with anti-PcrV and -PscF mAbs with T3SS-inhibitory
159 activity, we first evaluated in ELISA the reactivity of sera from a cohort of CF patients
160 that were chronically colonized with *P. aeruginosa* against recombinant PcrV and PscF
161 before testing them in functional assays (Figure 1A). Among the 34 sera tested, donors
162 16 and 25 exhibited the strongest reactivity for both proteins (Figure 1B).

163 To assess the capacity of serum-purified IgGs to block T3SS effector
164 translocation, we used a previously developed cellular model that is based on the
165 T3SS-dependent translocation of the ExoS effector fused to β-lactamase, ExoS-Bla
166 (Verove et al., 2012). Briefly, epithelial cells were exposed to *P. aeruginosa* CHA∆*exoS*
167 expressing the ExoS-Bla reporter in the presence of patients' polyclonal purified IgGs.
168 ExoS-Bla translocation was measured by monitoring fluorescence of the β-lactamase
169 FRET-competent substrate CCF2-AM, and expressed as normalized reporter injection.
170 Polyclonal IgGs from donors 16 and 25 showed a potent ExoS-Bla translocation
171 blocking activity with an almost complete inhibition of injection at 160 µg/mL (Figure
172 1C). To investigate whether the observed activity was driven by anti-PcrV and/or anti-
173 PscF specific IgGs, we absorbed specific Abs on beads coated with recombinant PcrV
174 or PscF to obtain polyclonal IgG samples depleted of the corresponding specific IgGs
175 (Figure 1D, top). The T3SS blocking activity of depleted polyclonal IgGs was then
176 evaluated using the same method as above (Figure 1D, bottom). The results showed
177 a decrease in inhibitory activity when anti-PcrV Abs were depleted from donor 25's
178 IgGs and when anti-PscF Abs were depleted from donor 16's IgGs, suggesting the
179 presence of inhibitory Abs against the respective proteins. Additionally, the findings
180 demonstrated that our recombinant antigen baits could effectively bind T3SS-inhibitory
181 Abs and could therefore be used to isolate memory B cells producing the
182 corresponding IgGs.

183

184 **Isolation of PcrV and PscF mAbs using a single cell direct sorting approach**

185 To isolate mAbs specific to PcrV and PscF, PBMCs were purified from whole
186 blood from the two selected donors. Next, using single cell sorting, IgG positive
187 memory B cells were isolated based on their ability to recognize either PscF or PcrV
188 (Figure 2A) and seeded at the frequency of one cell per well. Variable heavy and light
189 chain gene sequences were retrieved from isolated B cells leading to the production of
190 a total of 66 recombinant mAbs (53 and 13 putative anti-PscF and anti-PcrV,
191 respectively). The specific binding capacities of 10 anti-PscF and 4 anti-PcrV mAbs
192 were confirmed by ELISA against the corresponding recombinant proteins. EC_{50}
193 values calculated from ELISA data showed variable apparent affinities ranging from
194 ~50 µg/mL to 0.02 µg/mL (Figure 2B). Isolated mAbs originated from a variety of
195 variable gene germline families, as determined using the international immunogenetics
196 information system (IMGT) database alignments, and did not present any notable
197 features in term of mutation rates or HCDR3 length (Supplementary Table 1), with no
198 particular enrichment noted.

199 The ability of ELISA-confirmed anti-PscF and anti-PcrV mAbs to block T3SS-
200 mediated activity at a concentration of 100 µg/mL was subsequently evaluated using
201 the ExoS-Bla reporter system. No significant reduction in ExoS-Bla injection was
202 observed for any of the anti-PscF mAbs tested. However, two out of four anti-PcrV
203 mAbs, P5B3 and P3D6, significantly reduced ExoS-Bla injection, with P3D6 displaying
204 significantly stronger efficacy (Figure 2B).

205 To map the epitopes of the isolated mAbs, we next performed competition
206 ELISAs (Supplementary Table 2). Antibodies directed at PscF grouped into three
207 clusters, with P1D8 and P5G10 mAbs competing only against themselves. Similarly,
208 anti-PcrV mAbs also grouped into three clusters, with the two anti-PcrV mAbs
209 exhibiting T3SS inhibitory activity, P5B3 and P3D6, seemingly targeting overlapping
210 epitopes. Precise affinities of both mAbs were measured using biolayer interferometry
211 (BLI), revealing subnanomolar K_D values (Supplementary Table 3). Notably, P3D6
212 exhibited approximately 30-fold lower affinity compared to P3B3, despite
213 demonstrating greater efficacy in the inhibitory assay.

214

215 **P5B3 inhibits T3SS-dependent toxin injection by recognizing a highly conserved**
216 **epitope of PcrV**

217 Polymorphism in PcrV protein sequences was reported among *P. aeruginosa*
218 clinical isolates and should be considered in the development of therapeutic human
219 monoclonal Abs targeting PcrV (Figure 3A) (Tabor et al., 2018). To determine whether
220 the blocking activity of mAbs P5B3 and P3D6 was impacted by the PcrV sequence,
221 the reporter ExoS-Bla was introduced into a strain that lacked isogenic PcrV (Δ*pcrV*)
222 and synthetized the five most prevalent PcrV variants found in over 80% of clinical
223 isolates (Tabor et al., 2018). Monoclonal Ab P5B3 showed statistically significant T3SS
224 blocking activity towards all variants (Figure 3B) with estimated IC_{50} values of 100
225 μg/ml for variants 1, 2, 3, 4 and 400 μg/ml for variant 5 (Supplementary Figure 1). In
226 contrast, mAb P3D6 had no effect on variants 2, 3, 4 and 5, but strongly inhibited
227 variant 1 (Figure 3B) with an estimated IC_{50} of 3.7 μg/ml (Supplementary Figure 1),
228 indicating that the epitope recognized by P3D6 differs between PcrV variants.

229

230 **Anti-PcrV mAbs block translocon pore assembly**

231 It has been suggested that PcrV scaffolds the assembly of the PopB/PopD
232 translocon within host membranes by interacting with the PopD component of the pore
233 (Goure et al., 2004; Kundracik et al., 2022, 2022; Matteï et al., 2011). Furthermore,
234 polyclonal Abs raised against PcrV have been shown to inhibit the assembly of the
235 translocon in target membranes (Goure et al., 2005).

236 To investigate the mechanistic details of the inhibitory activity of mAbs P3D6
237 and P5B3, we used a *P. aeruginosa* strain deprived of all three T3SS effectors, ExoS,
238 ExoT and ExoY. This strain, named PAO1Δ3Tox (Cisz et al., 2008) harbors PcrV
239 variant 1 and provokes toxin-independent macrophage pyroptosis upon membrane
240 insertion of the PopB/PopD translocation pore (Dacheux et al., 2001). Death of J774
241 macrophages was monitored during 4h post-infection by measuring an increase in
242 propidium iodide fluorescence due to DNA binding to the nuclei of dead cells. Both
243 mAbs significantly reduced the cytotoxicity induced by PAO1Δ3Tox by 28% and 73%,
244 respectively (Figure 4A). Monoclonal Ab P3D6 exhibited a dose-response inhibition
245 with an estimated IC_{50} of 11.8 μg/mL (Figure 4B), while P5B3 did not exhibit a

246 significant dose-response effect at concentrations below 100 μg/mL (Figure 4C).
247 Overall, these results indicate that the binding of both mAbs to PcrV reduces the
248 formation of the translocation pore in target cell membranes, with P3D6 exhibiting more
249 potent activity.

250

251 **Crystal structure of PcrV* bound to Fab P3D6**

252 In order to identify the PcrV epitopes recognized by the two mAbs, we generated
253 a plasmid encoding a form of PcrV (PcrV*) amenable to crystallization (Tabor et al.,
254 2018) as well as Fab fragments from both P3D6 and P5B3 mAbs. PcrV* was
255 expressed in *E. coli* while both Fabs were expressed in HEK293F cells. Individual
256 proteins were purified by affinity and size-exclusion chromatographies. PcrV* was
257 incubated with either Fab fragment and samples were co-purified using size exclusion
258 chromatography. Despite the fact that both PcrV*-Fab P3D6 and PcrV*-Fab P5B3
259 complexes co-eluted in gel filtration, only the PcrV*-Fab P3D6 complex subsequently
260 generated diffracting crystals. Data were collected at the ESRF synchrotron in
261 Grenoble and the structure was solved by molecular replacement using Phaser
262 (McCoy et al., 2007). Iterative manual model building and model improvement led to
263 the structure whose statistics for data collection and refinement are presented in
264 Supplementary Table 4.

265 PcrV* is composed of six helices interwoven by loop regions. α-helices 1, 4 and
266 6 are the major secondary structure elements in PcrV*, while helices 2, 3 and 5 are 1-
267 or 2-turn helices. Most of the contacts formed between PcrV* and Fab P3D6 involve
268 Helix 6 and the loop preceding it (Figures 5A, 5B) and implicate a binding platform
269 made by both LC and HC from Fab P3D6. From the PcrV side, the interaction region
270 is highly polar, being formed by the side chains of Lys208, Gln217, Glu220, Lys222,
271 Ser225, Asp 226, Tyr 228, Glu231, Asn234, Thr243, Asp246 and Arg247. The
272 substitution of Ser225 in PcrV variant V1 by Lys or Arg in variants V2 to V5 is consistent
273 with P3D6 being inefficient on strains harboring these four variants.

274 In order to understand the protective role of mAb P3D6 in the context of the
275 PcrV pentameric oligomer located at the tip of the PscF needle, we generated a model
276 using the cryo-EM structure of the SipD pentamer (Guo and Galán, 2021) and aligned
277 our co-crystal structure onto this model (Figures 5C, 5D).This analysis revealed that

278 Fab P3D6 can successfully bind to one PcrV monomer (dark red and orange in Figure
279 5, respectively), but would be unable to bind to a pre-formed PcrV pentamer due to the
280 generation of clashes with neighboring subunits of the oligomeric form (Figure 5; the
281 structure of the Fab can be seen overlaid with that of the pentamer subunits).

282

283 **DISCUSSION**

284 We generated a panel of anti-PscF and -PcrV human mAbs through specific
285 memory B cell sorting from selected individuals. Although adsorption experiments with
286 recombinant PscF suggested the presence of anti-PscF Abs with T3SS inhibitory
287 activity in the donor from whom they were isolated, none of the isolated mAbs exhibited
288 this activity. Competition mapping showed that the anti-PscF mAbs targeted three
289 distinct regions of PscF, none of which seemingly involved in inhibitory activity. Further
290 epitope mapping would be necessary to gain deeper insight; however, in the absence
291 of a PscF structure, this remains challenging. Isolating a greater number of mAbs from
292 a selected donor with strong anti-PscF inhibitory activity would certainly increase the
293 likelihood of identifying one with T3SS-inhibiting properties.

294 Of the four anti-PcrV mAbs isolated, two exhibited T3SS inhibitory capacity.
295 Their mechanism of action could potentially involve (i) prevention of effector secretion
296 by acting as a cap for PcrV; (ii) prevention of effector translocation towards the host
297 cell by disruption of the PcrV-PopB/PopD interaction; or (iii) prevention of
298 oligomerization of PcrV itself(Gébus et al., 2009; Sawa et al., 2019). Here, we
299 measured the ability of the inhibiting anti-PcrV mAbs we isolated to block PopB/PopD
300 pore formation and toxin injection, and carried out a mechanistic and structural analysis
301 of their activity, in parallel with other mAbs targeting PcrV.

302 We set out to investigate and compare the mechanism of action of several anti-
303 PcrV mAbs: P3D6 mAb and P5B3 (this work), 30-B8 (Simonis et al., 2023), as well as
304 a previously reported humanized, bivalent PcrV-Psl mAb (DiGiandomenico et al.,
305 2014). In order to do so, we produced mAb 30-B8 and subsequently purchased mAb
306 MEDI3902 from MedChem. The P3D6, P5B3, 30-B8 and MEDI3902 mAbs were
307 notably compared by employing two assays capable of detecting T3SS inhibition, each
308 with a different readout: injection of the ExoS-Bla reporter into epithelial cells and
309 cytotoxicity measurements in macrophages as a read-out for translocon assembly. In

310 addition, we performed structural analyses on three of the mAb-PcrV complexes, from
311 the viewpoints of recognition of both monomeric and pentameric forms of PcrV.

312 Both MEDI3902 and 30-B8 mAbs potently inhibited the injection of ExoS-Bla
313 into target cells, with IC_{50} values of 117 ng/ml and 21.3 ng/ml, respectively (Figure 6A).
314 Monoclonal Abs isolated in this study also inhibited toxin injection, although
315 significantly less potently, with IC_{50} values of 3.65 µg/mL for P3D6, and around 100
316 µg/mL for P5B3. Monoclonal Ab MEDI3902 had previously been shown to bind to
317 different PcrV variants (Tabor et al., 2018) and here we confirmed that mAb 30-B8 was
318 similarly efficient at inhibiting toxin injection by strains carrying five different PcrV
319 variants (Simonis et al., 2023) (Supplementary Figure 2). Monoclonal Ab P5B3 was
320 also able to inhibit all variants, but only at high concentrations, while P3D6 was only
321 active against variant V1. Therefore, P5B3 appears to recognize a highly conserved
322 epitope whereas P3D6 seems to bind an overlapping epitope that includes the variable
323 Ser225, as suggested by the ELISA mapping competition and structural data, but does
324 so in a more effective manner.

325 In the macrophage cytotoxicity assay, translocon assembly was inhibited by
326 mAbs 30-B8 (IC_{50} of 45.2 ng/ml) and P3D6 (IC_{50} of 11.8 µg/mL), while P5B3 and
327 MEDI3902 did not exhibit significant dose-response inhibition. Together, these results
328 suggest that the T3SS-inhibiting activity of these anti-PcrV Abs may occur through
329 distinct mechanisms.

330 In order to understand the differences in potency and potentially in mechanisms
331 of action at a structural level, we compared the Fab-PcrV interaction regions for the
332 P3D6, 30-B8 and MEDI3902 Fabs. Monomeric PcrV is an elongated, dumbbell-shaped
333 molecule, and the chimeric form used in this study displays the same characteristics
334 (Figure 5A). Fab MEDI3902 binds to one of the extremities of monomeric PcrV,
335 extending in the longitudinal axis of the molecule (Figure 6B, top). This mode of binding
336 is distinct from that of 30-B8 and P3D6 Fabs, both of which recognize the C-terminal
337 region of PcrV (Figure 6B, middle) (Simonis et al., 2023). Therefore, the binding region
338 of 30-B8 and P3D6 does not, by itself, appear to explain the significant difference in
339 potency between the two mAbs. Moreover, a difference in affinity does not account for
340 the difference in potency either, as both mAbs bind to recombinant monomeric PcrV
341 with comparable apparent affinities of around 30 ng/ml (our data and Simonis et al.,
342 2023).

343 In order to perform this comparative analysis in the context of a PcrV oligomer,
344 we employed the model of the PcrV pentamer generated as described above, which
345 was based on the cryo-EM structure of SipD from *S. typhimurium* (Guo and Galán,
346 2021). According to this analysis, the only Fab that is able to bind to all PcrV protomers
347 in the pentamer without generating clashes with either PcrV or other Fabs is 30-B8
348 (Figure 6). In the case of MEDI3902, the Fab can bind the oligomer, but only with a 1:5
349 stoichiometry, due to possibility of clashes between Fabs. Finally, P3D6 is unable to
350 bind to a pre-formed pentamer, and can only recognize a PcrV protomer in its
351 monomeric form.

352 This structural analysis suggests different potential mechanisms of action. For
353 P3D6, the inability to bind to the pentamer points towards a mechanism involving
354 inhibition of oligomerization. Indeed, the analysis shows that binding of P3D6 to a
355 single PcrV monomer prevents the association of additional PcrV protomers through
356 Fab-protomer direct clashes. A similar mechanism of action may be suggested for
357 MEDI3902, as Fab-bound PcrV protomers cannot oligomerize, in this case due to
358 clashes between the Fabs themselves (Fig. 6). However, the fact that MEDI3902 does
359 not appear to prevent translocon insertion suggests that such a mechanism is unlikely
360 for this mAb as PcrV oligomerisation is required at the tip of the needle for translocon
361 assembly. In contrast to P3D6, MEDI3902 can bind the oligomerized PcrV pentamer
362 (with a stoichiometry of one) and its mechanism of action may thus be related to this
363 ability. Our results suggest that when MEDI3902 is bound to the PcrV oligomer, the
364 formation of the pore is not efficiently blocked while toxin injection is strongly inhibited
365 (Fig. 6). Therefore, the presence of one MEDI3902 Ab molecule at the tip of the needle
366 does not appear to efficiently prevent either the secretion of the translocator proteins
367 PopB/PopD through the needle, nor the interactions between PcrV and PopB/PopD,
368 which have been described as required for pore formation (Kundracik et al., 2022).
369 However, the MEDI3902 Ab molecule, seems to interfere with further interactions
370 between PcrV and the PopB/PopB complex, or with the sensing by PcrV of the host
371 cell, both of which are needed for toxin injection (Lee et al., 2010).

372 Lastly, 30-B8, which can bind the formed pentamer with a stoichiometry of five,
373 appears to be the most effective at blocking both pore formation and toxin injection.
374 The fact that the PcrV-bound 30-B8 Ab probably projects towards the cell membrane,

375 associated with its ability to bind to the PcrV pentamer at full occupancy, may result in
376 remarkable efficacy in blocking the interactions between PcrV and PopB/PopD.

377 In conclusion, here we show that patients with chronic infection with *P.*
378 *aeruginosa* can elicit anti-PscF and anti-PcrV mAbs that recognize different regions
379 within these proteins. Anti-PcrV Abs can act as T3SS inhibitors through different
380 mechanisms, with some exhibiting significantly greater efficacy than others. The
381 strategy employed here, involving the analysis of structural and functional data on anti-
382 T3SS mAbs should open new avenues towards deciphering the mechanism of T3SS
383 toxin translocation and enable the isolation of more effective mAbs targeting a broad
384 range of clinical strains.

385

386 **MATERIALS and METHODS**

387 **Clinical sample collection**

388 The study was approved by the French ethics committee (ID-RCB 2020-
389 A00311-38) and was carried out according to the Declaration of Helsinki, Good Clinical
390 Practice (GCP) guidelines and current French regulations. Written consent for
391 participation was not required for this study. The first phase was a non-interventional
392 study involving data and samples from human participants conducted according to
393 Reference Methodology No. 004 issued by French authorities (Commission Nationale
394 de l'Informatique et des Libertés). Screening and functional assays were performed on
395 human sera previously collected at Grenoble Alpes University Hospital (France), from
396 CF patients chronically infected with *P. aeruginosa*. Participants were all informed and
397 did not object to this phase of the study. Inclusion criteria for the second phase of the
398 study were: patients with positive screening during phase one, ≥ 18 years old, ≥32 Kg,
399 with a programmed blood sampling at Grenoble Alpes University Hospital and not
400 being opposed to the second phase of the project. Whole blood was then collected
401 using BD Vacutainer® EDTA tubes (Becton Dickinson) and PBMCs were purified by
402 density gradient centrifugation using Lymphoprep (Eurobio scientific) following
403 manufacturing guidelines. Cells were then stored in liquid nitrogen until further use.

404

405 **Bacterial strains, genetic manipulations and growth conditions**

406 *P. aeruginosa* strains used in this study are listed in Supplementary Table 5.
407 Strains were cultured in LB media at 37 °C. For infection experiments, bacteria were
408 grown until the measured optical density at 600 nm (OD_{600nm}) of 1. The genes
409 encoding the most common variants of PcrV were cloned into the *Pseudomonas*
410 replicative vector derived from pUCP21 (West et al., 1994) containing the P*pcrG*
411 promoter driving the *pcrGVHpopDB* operon expression (West et al., 1994). The
412 plasmids, kindly provided by Simona Barzu (Sanofi Pasteur, Lyon), were
413 transformed into the *P. aeruginosa* strain CHA lacking *pcrV* (Goure et al., 2004).
414

415 **Expression and purification of full length PcrV and PcrV***

416 Expression of full-length PcrV from strain PAO1, cloned into a pET15b vector,
417 was performed in *E. coli* BL21(DE3) as previously described, with small modifications
418 (Nanao et al., 2003). Expression was induced with 1mM of Isopropyl β-D-1-
419 thiogalactopyranoside (IPTG) at OD_{600} = 0.8 AU and cells were then grown overnight
420 at 20°C with shaking at 250 rpm. Cells were harvested by centrifugation and lysed by
421 passing through a French Press 3 times at 25 Kpsi in lysis Buffer (50 mM Tris pH8,
422 200 mM NaCl, 20 mM Imidazole) supplemented with a protein inhibitor cocktail tablet
423 (ROCHE). The supernatant was cleared by centrifugation at 18,000 rpm and
424 subsequently loaded onto Ni-IDA resin (Macherey-Nagel). The resin was washed with
425 lysis buffer and the sample was eluted with lysis buffer supplemented with 100 mM
426 imidazole. Fractions containing the sample were pooled and applied to a size-
427 exclusion chromatography column (Superdex 200 HiLoad 16/600) pre-equilibrated in
428 SEC buffer (20mM Tris pH 8, 150 mM NaCl, 1 mM EDTA). A chimeric form of PcrV
429 (PcrV*) consisting of amino acids 1-17 fused to 136-249, was constructed based on a
430 construct made by Tabor et al. (2018) and employed for crystallization purposes. The
431 purification protocol was the same as above, the only difference being that 250 mM
432 imidazole was employed to elute the sample from the Ni resin.

433

434 **Expression and purification of PscF**

435 Expression of PscF from strain PAO1 was performed in *E. coli* BL21(DE3)
436 grown in Terrific Broth. Expression was induced with 1 mM Isopropyl β-D-1-
437 thiogalactopyranoside (IPTG) at OD_{600} = 0.6 AU and cells were then grown for an

438 additional 3 hours at 37 °C with shaking at 250 rpm. Cells were harvested by
439 centrifugation and lysed by passing through a French Press 3 times at 25 kpsi in lysis
440 buffer (50 mM Tris pH 8, 200 mM NaCl, 20 mM Imidazole, 2 % glycerol) supplemented
441 with a protein inhibitor cocktail tablet (Roche). The supernatant was cleared by
442 centrifugation at 18,000 rpm and applied to a Ni-IDA resin (Macherey-Nagel). The resin
443 was washed with lysis buffer and the protein was eluted with lysis buffer supplemented
444 with 250 mM imidazole. Fractions were then buffer exchanged in an Amicon Ultra 10
445 kDa cutoff concentrator against a buffer exempt of imidazole (50 mM Tris pH 8, 200
446 mM NaCl, 2 % glycerol).

447

448 **ELISA assays**

449 For direct ELISA assays, serial dilutions of sera or mAbs were transferred in
450 antigen-adsorbed wells of 96-well plates. Antigen binding was detected by an alkaline
451 phosphatase-conjugated goat anti-human immunoglobulin G (IgG) F(ab′)2 Ab
452 (Jackson Immuno). For competition ELISA, serial dilution of competitor mAbs were
453 transferred in antigen-adsorbed wells. Following an incubation of 30 min, biotinylated
454 mAbs were added to the wells at a concentration corresponding to the EC_{70} (Effective
455 concentration 70). Biotinylated mAbs were detected using alkaline phosphatase
456 conjugated streptavidin. Polyclonal Abs raised in rabbits against PscF and PcrV
457 (Goure et al., 2004) were used as positive controls.

458

459 **Sorting of specific memory B cells**

460 Briefly, PBMCs were stained for 30 min at 4ºC in the dark, using Facs-Buffer
461 (PBS-1X 0,5 % BSA , 2mM EDTA) with Live Dead staining (Thermo L34957), Anti-
462 human CD3-Vio-Blue (Miltenyi 130-114-519), Anti-human CD20 Pe-Vio707 (Miltenyi
463 130-111-345), Anti-human CD19 Pe-Vio707 (Miltenyi 130-113-649), Anti-human IgM
464 PE (Miltenyi 130-093-075), Anti-human IgA PE (Miltenyi 130-113-476), Anti-human
465 IgD PE (Miltenyi 130-110-643), Anti-human CD27 APC (Miltenyi 130-108-336), in the
466 presence of recombinant biotinylated His-PcrV-Avitag coupled with streptavidin
467 BUV737 (BD 612775) or streptavidin Vio-515 (Miltenyi 103-107-459), and
468 recombinant biotinylated His-PscF-Avitag coupled with streptavidin BUV496 (BD

469 612961) or streptavidin BV605 (Biolegend 405229). After washing, the cells were
470 resuspended in Facs-Buffer and PscF or PcrV positive B cells are sorted and clonally
471 seeded in 96 plates containing lysis buffer using BD FACSAria Fusion cytometer (BD
472 Biosciences).

473

474 **Isolation and production of mAbs**

475 Sequences coding for variable regions of both heavy and light (κ and λ) chains
476 were isolated by reverse transcription on total mRNA followed by a multiplex nested
477 PCR using a set of primers covering the diversity of V-region diversity. V-regions family
478 was attributed after sequencing of amplicons and alignment in the IMGT database
479 (https://imgt.org). An additional round of PCR using primers specific to the identified
480 family was performed followed by the cloning of V-regions genes in corresponding
481 vectors containing IgG1H, IgGκ and IgGλ constant regions. MAbs were recovered by
482 transient transfection in HEK293F cells (ThermoFisher scientific) and purification by
483 affinity chromatography using Protein A Sepharose (Sigma). Regarding 30-B8, the
484 sequences coding for the variable regions of heavy and light chains were synthesized
485 by Eurofins according to the sequence published by Simonis and coworkers (Simonis
486 et al., 2023). Cloning and production were performed as described above.

487

488 **P3D6 and P5B3 Fab production**

489 Sequences coding for Fab fragments were obtained by inserting stop codons
490 on genes corresponding to heavy chains of the mAbs by PCR using site directed
491 mutagenesis (Quickchange II, Agilent) according to manufacturer's instructions.
492 Mutated heavy and corresponding light chain genes were cloned into appropriate
493 expression plasmids for eukaryotic cell expression and were co-transfected at a 2:1
494 ration into FreeStyle 293-F cells (ThermoFisher). Fabs were purified using
495 KappaSelect affinity chromatography (Cytiva).

496

497 **Cellular tests for T3SS activity**

498 *ExoS-Bla translocation*

499 The T3SS-dependent toxin injection into epithelial A549 cells was measured
500 using the reporter system based on Bla/CCF2 enzyme/substrate combination
501 (Charpentier and Oswald, 2004) previously described for *P. aeruginosa* (Verove et
502 al., 2012). *P. aeruginosa* strain CHAΔ*exoS* carring ExoS-Bla fusion on the
503 chromosome was used to infect A549 cells at the multiplicity of infection (MOI) of 5.
504 The level of injected ExoS-β-lactamase was measured using CCF2 substrate, as
505 described previously (Verove et al., 2012). All values were normalized using non-
506 infected cells and cells infected in the absence of Abs as references.
507
508 *Pore formation / propidium iodide incorporation into macrophages*
509 To assess the formation of a T3SS translocation pore, macrophages were
510 infected with a *P. aeruginosa* strain PAO1Δ3Tox devoid of three exotoxins (Cisz et al.,
511 2008). Two days before the experiment, J774 cells were seeded in a 96-well plate
512 (Greiner, 655090) at a density of 100 000 cells per well in DMEM supplemented with
513 10% FCS. The day before the experiment, the strain was grown overnight in LB
514 medium. The next day, bacteria were sub-cultures in fresh LB media until an OD_{600nm}
515 of 1 and the macrophages were washed two times with PBS before addition of 65 µL
516 of DMEM 10% FCS containing 2 µg/mL of Propidium Iodide. Antibodies diluted in
517 DMEM, 10% FCS (25 µL) were then added followed by 10 µL of bacteria diluted in
518 DMEM 10% FCS to give a MOI of 5. Propidium iodide fluorescence was recorded in a
519 Fluoroskan fluorimeter every 10 minutes. The data of each fluorescence kinetics of the
520 triplicates were processed in R Studio to calculate the Area Under the Curve, as
521 described before (Ngo et al., 2019). This metrics was then normalized using non-
522 infected cells and cells infected in the absence of Abs as references.
523
524 **Data processing and analysis**
525 Data from independent cell experiments were pooled and analyzed in R Studio
526 by one-way ANOVA followed by paired t-test or Kuskal-Wallis followed by the Dunn
527 test. Dose-response fitting was performed using the drc package and logistic models.
528
529 **Bio-layer interferometry**
530 BLI experiments were performed on an OctetRED96e from Satorius/FortéBio
531 (former Pall/FortéBio) and were recorded with software provided by the manufacturer

532 (Data Acquisition v11.1). All protein samples were diluted in analysis buffer (1X PBS
533 pH 7.4, 0.02% Tween-20). 10 mM glycine pH 2.0 was used as regeneration buffer.
534 Commercial SA or SAX (streptavidin) biosensors (Pall/FortéBio) were used to capture
535 biotinylated PcrV. Kinetic analyses were performed in black 96-well plates (Nunc F96
536 MicroWell, Thermo Fisher Scientific) at 25°C with agitation at 1000 rpm. After
537 incubation and equilibration of biosensors in analysis buffer, PcrV samples were
538 applied at a concentration of 2.5 mg/ml by dipping biosensors until reaching a spectrum
539 shift between 1.2 and 2 nm, followed by an additional equilibration step in analysis
540 buffer. For association measurements, all analyte samples were diluted in analysis
541 buffer at concentrations either between 3.12 and 200 nM for IgGs or between 50 and
542 3200 nM for Fab fragments. Association phases were monitored while dipping the
543 functionalized biosensors in analyte solutions for 5 min after recording a baseline for 2
544 min, and the dissociation phases monitored in analysis buffer for 10min. To assess
545 and monitor unspecific binding of analytes, measurements were performed with
546 biosensors treated with the same protocols but replacing ligand solutions with analysis
547 buffer. All measurements were performed in duplicate using sample preparations.
548 Kinetic data were processed with software provided by the manufacturer (Data
549 analysis HT v11.1). Signals from zero-concentration samples were subtracted from the
550 signals obtained for each functionalized biosensor and each analyte concentration.
551 Resulting specific kinetics signals were then fitted using a global fit method and 1:2
552 bivalent analyte model for full Abs/IgG and 1:1 Langmuir model for Fab. Reported
553 kinetics parameter values were obtained by averaging the values obtained with
554 duplicated assays and reported errors as the standard deviation.
555

556 **Crystallization of the PcrV*-Fab P3D6 complex**

557 PcrV* and P3D6 Fab were mixed in a 1:2 ratio for 1 hr at room temperature prior
558 to being subjected to size exclusion chromatography using a Superdex 200 10/300GL
559 increase column in SEC buffer (20 mM Tris pH 7.4, 150 mM NaCl, 1 mM EDTA). Peaks
560 harboring PcrV*:Fab complexes in SDS-PAGE were pooled, concentrated and used
561 for crystallization trials using the ISBG HTX crystallization platform in Grenoble. Initial
562 crystallization conditions were optimized manually (25 % PEG 1000, 1mM $ZnCl_2$, 100
563 mM sodium acetate pH 5.5), and diffracting crystals were obtained using microseeding.
564 All crystals were grown using the hanging drop vapor diffusion method at 20 °C. Single

565 crystals were mounted in cryo-loops and flash cooled in liquid nitrogen. X-ray diffraction
566 data were collected under a nitrogen stream at 100° K at the European Synchrotron
567 Facility (ESRF, Grenoble, France).

568

569 **Structure determination and refinement**

570 The best diffraction data were collected to 2.56 Å on beamline ID30A-1 (ESRF)
571 (Bowler 2015). The diffracting crystal was in space group $P2_1$ and displayed one 1:1
572 PcrV:Fab complex per asymmetric unit. Statistics on data collection and refinement
573 are summarized in supplementary table 5. X-ray diffraction images were indexed and
574 scaled with XDS (Kabsch 2010). ADXV ("Arvai, A. (2020). ADXV. A Program to Display
575 X-ray Diffraction Images. https://www.scripps.edu/tainer/arvai/adxv.html," n.d.) and
576 XDSGUI (Brehm et al., 2023) were used to perform data quality and resolution cutoff
577 check-ups (Karplus and Diederichs, 2015). The maximum possible resolution was
578 determined using the STARANISO server (Tickle, 2007). The reduced X-ray diffraction
579 data was imported into the CCP4 program suite (Agirre et al., 2023). The PcrV*-Fab
580 P3D6 structure was solved by molecular replacement using PHASER (McCoy et al.,
581 2007) and an AlphaFold2 ColabFold-generated model (Mirdita et al., 2022). The PcrV*
582 and Fab model chains were placed sequentially. The structure was completed by
583 cycles of manual model building with COOT (Emsley and Cowtan, 2004, p. 200). Water
584 molecules were added to the residual electron density map as implemented in COOT.
585 Crystallographic macromolecular refinement was performed with REFMAC
586 (Murshudov et al., 2011). Cycles of model building and refinement were performed
587 until R_{work} and R_{free} converged. The TLS definition was determined and validated using
588 the TLSMD (Painter and Merritt, 2006) and PARVATI (Zucker et al., 2010) servers.
589 The stereochemical quality of the refined models was verified with MOLPROBITY
590 (Chen et al., 2010, p. 20), PROCHECK (Laskowski et al., 1993) and PDB-REDO
591 (Joosten et al., 2014). Secondary structure assignment was performed by DSSP
592 (Kabsch and Sander, 1983) and STRIDE (Heinig and Frishman, 2004). Figures
593 displaying protein structures were generated with PYMOL (http://www.pymol.org).

594

595

ACKNOWLEDGEMENTS

This work was supported by a grant from the Agence Nationale de la Recherche (ANR-22-CE18-0009) to PP, AD and IA, as well as grant 183360 from the Région Auvergne Rhône-Alpes to PP and AD. This work used the platforms of the Grenoble Instruct-ERIC center (ISBG; UAR 3518 CNRSCEA-UGA-EMBL) within the Grenoble Partnership for Structural Biology (PSB), supported by FRISBI (ANR-10-INBS-0005-02) and GRAL, financed within the University Grenoble Alpes graduate school (Ecoles Universitaires de Recherche) CBH-EUR-GS (ANR-17-EURE-0003). The IBS acknowledges integration into the Interdisciplinary Research Institute of Grenoble (CEA).

DATA AVAILABILITY

All data generated or analyzed during this study are included in the manuscript and supporting files, with the exception of the final refined model coordinates and structure factors corresponding to the PcrV*- Fab P3D6 complex. Those were deposited in the Protein Data Bank (PDB, http://www.rcsb.org), ID code: 9FM0.

612 **REFERENCES**

613 Agirre J, Atanasova M, Bagdonas H, Ballard CB, Baslé A, Beilsten-Edmands J, Borges
614 RJ, Brown DG, Burgos-Mármol JJ, Berrisford JM, Bond PS, Caballero I, Catapano L,
615 Chojnowski G, Cook AG, Cowtan KD, Croll TI, Debreczeni JÉ, Devenish NE, Dodson
616 EJ, Drevon TR, Emsley P, Evans G, Evans PR, Fando M, Foadi J, Fuentes-Montero
617 L, Garman EF, Gerstel M, Gildea RJ, Hatti K, Hekkelman ML, Heuser P, Hoh SW,
618 Hough MA, Jenkins HT, Jiménez E, Joosten RP, Keegan RM, Keep N, Krissinel EB,
619 Kolenko P, Kovalevskiy O, Lamzin VS, Lawson DM, Lebedev AA, Leslie AGW,
620 Lohkamp B, Long F, Malý M, McCoy AJ, McNicholas SJ, Medina A, Millán C, Murray
621 JW, Murshudov GN, Nicholls RA, Noble MEM, Oeffner R, Pannu NS, Parkhurst JM,
622 Pearce N, Pereira J, Perrakis A, Powell HR, Read RJ, Rigden DJ, Rochira W, Sammito
623 M, Sánchez Rodríguez F, Sheldrick GM, Shelley KL, Simkovic F, Simpkin AJ, Skubak
624 P, Sobolev E, Steiner RA, Stevenson K, Tews I, Thomas JMH, Thorn A, Valls JT, Uski
625 V, Usón I, Vagin A, Velankar S, Vollmar M, Walden H, Waterman D, Wilson KS, Winn
626 MD, Winter G, Wojdyr M, Yamashita K. 2023. The *CCP* 4 suite: integrative software
627 for macromolecular crystallography. *Acta Crystallogr D Struct Biol* **79**:449–461.
628 doi:10.1107/S2059798323003595

629 Arvai, A. (2020). ADXV. A Program to Display X-ray Diffraction Images.
630 https://www.scripps.edu/tainer/arvai/adxv.html. n.d.

631 Berube BJ, Murphy KR, Torhan MC, Bowlin NO, Williams JD, Bowlin TL, Moir DT,
632 Hauser AR. 2017. Impact of Type III Secretion Effectors and of Phenoxyacetamide
633 Inhibitors of Type III Secretion on Abscess Formation in a Mouse Model of
634 Pseudomonas aeruginosa Infection. *Antimicrob Agents Chemother* **61**:e01202-17.
635 doi:10.1128/AAC.01202-17

636 Bowlin NO, Williams JD, Knoten CA, Torhan MC, Tashjian TF, Li B, Aiello D, Mecsas
637 J, Hauser AR, Peet NP, Bowlin TL, Moir DT. 2014. Mutations in the Pseudomonas
638 aeruginosa Needle Protein Gene *pscF* Confer Resistance to Phenoxyacetamide
639 Inhibitors of the Type III Secretion System. *Antimicrob Agents Chemother* **58**:2211–
640 2220. doi:10.1128/AAC.02795-13

641 Brehm W, Triviño J, Krahn JM, Usón I, Diederichs K. 2023. *XDSGUI* : a graphical user
642 interface for *XDS* , *SHELX* and *ARCIMBOLDO*. *J Appl Crystallogr* **56**:1585–1594.
643 doi:10.1107/S1600576723007057

644 Charpentier X, Oswald E. 2004. Identification of the Secretion and Translocation
645 Domain of the Enteropathogenic and Enterohemorrhagic *Escherichia coli* Effector Cif,
646 Using TEM-1 β-Lactamase as a New Fluorescence-Based Reporter. *J Bacteriol*
647 **186**:5486–5495. doi:10.1128/JB.186.16.5486-5495.2004

648 Chastre J, François B, Bourgeois M, Komnos A, Ferrer R, Rahav G, De Schryver N,
649 Lepape A, Koksal I, Luyt C-E, Sánchez-García M, Torres A, Eggimann P, Koulenti D,

650 Holland TL, Ali O, Shoemaker K, Ren P, Sauser J, Ruzin A, Tabor DE, Akhgar A, Wu
651 Y, Jiang Y, DiGiandomenico A, Colbert S, Vandamme D, Coenjaerts F, Malhotra-
652 Kumar S, Timbermont L, Oliver A, Barraud O, Bellamy T, Bonten M, Goossens H,
653 Reisner C, Esser MT, Jafri HS, The COMBACTE-MAGNET EVADE Study Group,
654 Joannidis M, Klimscha W, De Waele E, Devriendt J, Huberlant V, Depuydt P, Van
655 Boxstael S, Peric M, Kopic J, Hanauer M, Hruby T, Sramek V, Svoboda P, Vymazal T,
656 Novacek M, Annane D, Mira J-P, Souweine B, Dequin P-F, Meziani F, Stephan F,
657 Nseir S, Gibot S, Schwebel C, Plantefeve G, Diehl J-L, Richard C, Lamer C, Klouche
658 K, Jaber S, Zakynthinos E, Filntisis G, Zakynthinos S, Koutsoukou A, Saroglou G,
659 Nikolaou C, Vlachogianni G, Pnevmatikos I, Mandragos K, Kremer I, Rozgonyi ZD,
660 Marjanek Z, Martin-Loeches I, Singer P, Van Heerden V, Carmeli Y, Povoa P, Seoane
661 AA, Moura P, Gonzalez F, Ramirez P, Marti AT, Roca RF, Oteiza L, Escudero D,
662 Piacentini E, Vera P, Tamayo L, Gallego MAG, Canas BS, Figueira I, Leon R, Korten
663 V, Akova M, Wyncoll D, Whitehouse T, Hopkins P, Sim M, Golan Y, Zervos M, Vazquez
664 J, Cherabuddi K, Smulian G, Rouphael N, Welker J, Sims M, Van Duin D, McCarthy
665 T, Polk C. 2022. Safety, efficacy, and pharmacokinetics of gremubamab (MEDI3902),
666 an anti-Pseudomonas aeruginosa bispecific human monoclonal antibody, in P.
667 aeruginosa-colonised, mechanically ventilated intensive care unit patients: a
668 randomised controlled trial. *Crit Care* **26**:355. doi:10.1186/s13054-022-04204-9

669 Chen VB, Arendall WB, Headd JJ, Keedy DA, Immormino RM, Kapral GJ, Murray LW,
670 Richardson JS, Richardson DC. 2010. *MolProbity*: all-atom structure validation for
671 macromolecular crystallography. *Acta Crystallogr D Biol Crystallogr* **66**:12–21.
672 doi:10.1107/S0907444909042073

673 Cisz M, Lee P-C, Rietsch A. 2008. ExoS Controls the Cell Contact-Mediated Switch to
674 Effector Secretion in *Pseudomonas aeruginosa*. *J Bacteriol* **190**:2726–2738.
675 doi:10.1128/JB.01553-07

676 Coburn B, Sekirov I, Finlay BB. 2007. Type III Secretion Systems and Disease. *Clin*
677 *Microbiol Rev* **20**:535–549. doi:10.1128/CMR.00013-07

678 Crowe JE. 2022. Human Antibodies for Viral Infections. *Annu Rev Immunol* **40**:349–
679 386. doi:10.1146/annurev-immunol-042718-041309

680 Dacheux D, Goure J, Chabert J, Usson Y, Attree I. 2001. Pore-forming activity of type
681 III system-secreted proteins leads to oncosis of *Pseudomonas aeruginosa* -infected
682 macrophages. *Molecular Microbiology* **40**:76–85. doi:10.1046/j.1365-
683 2958.2001.02368.x

684 De Melo AG, Morency C, Moineau S. 2024. Virulence-associated factors as targets for
685 phage infection. *Current Opinion in Microbiology* **79**:102471.
686 doi:10.1016/j.mib.2024.102471

687 Derewenda ZS. 2011. It's all in the crystals…. *Acta Crystallogr D Biol Crystallogr*
688 **67**:243–248. doi:10.1107/S0907444911007797

689 Diepold A, Wagner S. 2014. Assembly of the bacterial type III secretion machinery.
690 *FEMS Microbiol Rev* **38**:802–822. doi:10.1111/1574-6976.12061

691 DiGiandomenico A, Keller AE, Gao Cuihua, Rainey GJ, Warrener P, Camara MM,
692 Bonnell J, Fleming R, Bezabeh B, Dimasi N, Sellman BR, Hilliard J, Guenther CM,
693 Datta V, Zhao W, Gao Changshou, Yu X-Q, Suzich JA, Stover CK. 2014. A
694 multifunctional bispecific antibody protects against *Pseudomonas aeruginosa*. *Sci*
695 *Transl Med* **6**. doi:10.1126/scitranslmed.3009655

696 Dortet L, Lombardi C, Cretin F, Dessen A, Filloux A. 2018. Pore-forming activity of the
697 Pseudomonas aeruginosa type III secretion system translocon alters the host
698 epigenome. *Nat Microbiol* **3**:378–386. doi:10.1038/s41564-018-0109-7

699 Duan L, Zhang J, Chen Z, Gou Q, Xiong Q, Yuan Y, Jing H, Zhu J, Ni L, Zheng Y, Liu
700 Z, Zhang X, Zeng H, Zou Q, Zhao Z. 2021. Antibiotic Combined with Epitope-Specific
701 Monoclonal Antibody Cocktail Protects Mice Against Bacteremia and Acute
702 Pneumonia from Methicillin-Resistant Staphylococcus aureus Infection. *JIR* **Volume**
703 **14**:4267–4282. doi:10.2147/JIR.S325286

704 Emsley P, Cowtan K. 2004. *Coot* : model-building tools for molecular graphics. *Acta*
705 *Crystallogr D Biol Crystallogr* **60**:2126–2132. doi:10.1107/S0907444904019158

706 Erskine PT, Knight MJ, Ruaux A, Mikolajek H, Sang NWF, Withers J, Gill R, Wood SP,
707 Wood M, Fox GC, Cooper JB. 2006. High Resolution Structure of BipD: An Invasion
708 Protein Associated with the Type III Secretion System of Burkholderia Pseudomallei.
709 *Journal of Molecular Biology* **363**:125–136. doi:10.1016/j.jmb.2006.07.069

710 Faudry E, Vernier G, Neumann E, Forge V, Attree I. 2006. Synergistic Pore Formation
711 by Type III Toxin Translocators of *Pseudomonas aeruginosa*. *Biochemistry* **45**:8117–
712 8123. doi:10.1021/bi060452+

713 François B, Luyt C-E, Dugard A, Wolff M, Diehl J-L, Jaber S, Forel J-M, Garot D, Kipnis
714 E, Mebazaa A, Misset B, Andremont A, Ploy M-C, Jacobs A, Yarranton G, Pearce T,
715 Fagon J-Y, Chastre J. 2012. Safety and pharmacokinetics of an anti-PcrV PEGylated
716 monoclonal antibody fragment in mechanically ventilated patients colonized with
717 Pseudomonas aeruginosa: A randomized,double-blind, placebo-controlled trial*.
718 *Critical Care Medicine* **40**:2320–2326. doi:10.1097/CCM.0b013e31825334f6

719 Frank DW, Vallis A, Wiener-Kronish JP, Roy-Burman A, Spack EG, Mullaney BP,
720 Megdoud M, Marks JD, Fritz R, Sawa T. 2002. Generation and Characterization of a
721 Protective Monoclonal Antibody to *Pseudomonas aeruginosa* PcrV. *J INFECT DIS*
722 **186**:64–73. doi:10.1086/341069

723 Gébus C, Faudry E, Bohn Y-ST, Elsen S, Attree I. 2009. Oligomerization of PcrV and
724 LcrV, protective antigens of Pseudomonas aeruginosa and Yersinia pestis. *Journal of*
725 *Biological Chemistry* **284**:21776. doi:10.1074/jbc.A803146200

726 Goure J, Broz P, Attree O, Cornelis GR, Attree I. 2005. Protective Anti-V Antibodies
727 Inhibit *Pseudomonas* and *Yersinia* Translocon Assembly within Host Membranes. *J*
728 *INFECT DIS* **192**:218–225. doi:10.1086/430932

729 Goure J, Pastor A, Faudry E, Chabert J, Dessen A, Attree I. 2004. The V Antigen of
730 *Pseudomonas aeruginosa* Is Required for Assembly of the Functional PopB/PopD
731 Translocation Pore in Host Cell Membranes. *Infect Immun* **72**:4741–4750.
732 doi:10.1128/IAI.72.8.4741-4750.2004

733 Guo EZ, Galán JE. 2021. Cryo-EM structure of the needle filament tip complex of the
734 *Salmonella* type III secretion injectisome. *Proc Natl Acad Sci USA* **118**:e2114552118.
735 doi:10.1073/pnas.2114552118

736 Habenstein B, El Mammeri N, Tolchard J, Lamon G, Tawani A, Berbon M, Loquet A.
737 2019. Structures of Type III Secretion System Needle Filaments In: Wagner S, Galan
738 JE, editors. Bacterial Type III Protein Secretion Systems, Current Topics in
739 Microbiology and Immunology. Cham: Springer International Publishing. pp. 109–131.
740 doi:10.1007/82_2019_192

741 Hauser AR. 2009. The type III secretion system of Pseudomonas aeruginosa: infection
742 by injection. *Nat Rev Microbiol* **7**:654–665. doi:10.1038/nrmicro2199

743 Heinig M, Frishman D. 2004. STRIDE: a web server for secondary structure
744 assignment from known atomic coordinates of proteins. *Nucleic Acids Research*
745 **32**:W500–W502. doi:10.1093/nar/gkh429

746 Horcajada JP, Montero M, Oliver A, Sorlí L, Luque S, Gómez-Zorrilla S, Benito N, Grau
747 S. 2019. Epidemiology and Treatment of Multidrug-Resistant and Extensively Drug-
748 Resistant Pseudomonas aeruginosa Infections. *Clin Microbiol Rev* **32**:e00031-19.
749 doi:10.1128/CMR.00031-19

750 Hu Y, Huang H, Cheng X, Shu X, White AP, Stavrinides J, Köster W, Zhu G, Zhao Z,
751 Wang Y. 2017. A global survey of bacterial type III secretion systems and their
752 effectors. *Environmental Microbiology* **19**:3879–3895. doi:10.1111/1462-2920.13755

753 Imamura Y, Yanagihara K, Fukuda Y, Kaneko Y, Seki M, Izumikawa K, Miyazaki Y,
754 Hirakata Y, Sawa T, Wiener-Kronish JP, Kohno S. 2007. Effect of anti-PcrV antibody
755 in a murine chronic airway Pseudomonas aeruginosa infection model. *European*
756 *Respiratory Journal* **29**:965–968. doi:10.1183/09031936.00147406

757 Jain R, Beckett VV, Konstan MW, Accurso FJ, Burns JL, Mayer-Hamblett N, Milla C,
758 VanDevanter DR, Chmiel JF. 2018. KB001-A, a novel anti-inflammatory, found to be

759 safe and well-tolerated in cystic fibrosis patients infected with Pseudomonas
760 aeruginosa. *Journal of Cystic Fibrosis* **17**:484–491. doi:10.1016/j.jcf.2017.12.006

761 Joosten RP, Long F, Murshudov GN, Perrakis A. 2014. The *PDB_REDO* server for
762 macromolecular structure model optimization. *IUCrJ* **1**:213–220.
763 doi:10.1107/S2052252514009324

764 Kabsch W, Sander C. 1983. Dictionary of protein secondary structure: Pattern
765 recognition of hydrogen-bonded and geometrical features. *Biopolymers* **22**:2577–
766 2637. doi:10.1002/bip.360221211

767 Karplus PA, Diederichs K. 2015. Assessing and maximizing data quality in
768 macromolecular crystallography. *Current Opinion in Structural Biology* **34**:60–68.
769 doi:10.1016/j.sbi.2015.07.003

770 Kaufmann SHE, Dorhoi A, Hotchkiss RS, Bartenschlager R. 2018. Host-directed
771 therapies for bacterial and viral infections. *Nat Rev Drug Discov* **17**:35–56.
772 doi:10.1038/nrd.2017.162

773 Kundracik E, Trichka J, Díaz Aponte J, Roistacher A, Rietsch A. 2022. PopB-PcrV
774 Interactions Are Essential for Pore Formation in the Pseudomonas aeruginosa Type III
775 Secretion System Translocon. *mBio* **13**:e02381-22. doi:10.1128/mbio.02381-22

776 La Guidara C, Adamo R, Sala C, Micoli F. 2024. Vaccines and Monoclonal Antibodies
777 as Alternative Strategies to Antibiotics to Fight Antimicrobial Resistance. *IJMS*
778 **25**:5487. doi:10.3390/ijms25105487

779 Laskowski RA, MacArthur MW, Moss DS, Thornton JM. 1993. PROCHECK: a program
780 to check the stereochemical quality of protein structures. *J Appl Crystallogr* **26**:283–
781 291. doi:10.1107/S0021889892009944

782 Lee P, Stopford CM, Svenson AG, Rietsch A. 2010. Control of effector export by the
783 *Pseudomonas aeruginosa* type III secretion proteins PcrG and PcrV. *Molecular*
784 *Microbiology* **75**:924–941. doi:10.1111/j.1365-2958.2009.07027.x

785 Levin MJ, Ustianowski A, De Wit S, Launay O, Avila M, Templeton A, Yuan Y,
786 Seegobin S, Ellery A, Levinson DJ, Ambery P, Arends RH, Beavon R, Dey K, Garbes
787 P, Kelly EJ, Koh GCKW, Near KA, Padilla KW, Psachoulia K, Sharbaugh A, Streicher
788 K, Pangalos MN, Esser MT. 2022. Intramuscular AZD7442 (Tixagevimab–Cilgavimab)
789 for Prevention of Covid-19. *N Engl J Med* **386**:2188–2200.
790 doi:10.1056/NEJMoa2116620

791 Lunelli M, Hurwitz R, Lambers J, Kolbe M. 2011. Crystal Structure of PrgI-SipD: Insight
792 into a Secretion Competent State of the Type Three Secretion System Needle Tip and
793 its Interaction with Host Ligands. *PLoS Pathog* **7**:e1002163.
794 doi:10.1371/journal.ppat.1002163

Matteï P, Faudry E, Job V, Izoré T, Attree I, Dessen A. 2011. Membrane targeting and pore formation by the type III secretion system translocon. *The FEBS Journal* **278**:414–426. doi:10.1111/j.1742-4658.2010.07974.x

McCoy AJ, Grosse-Kunstleve RW, Adams PD, Winn MD, Storoni LC, Read RJ. 2007. *Phaser* crystallographic software. *J Appl Crystallogr* **40**:658–674. doi:10.1107/S0021889807021206

Mirdita M, Schütze K, Moriwaki Y, Heo L, Ovchinnikov S, Steinegger M. 2022. ColabFold: making protein folding accessible to all. *Nat Methods* **19**:679–682. doi:10.1038/s41592-022-01488-1

Montagner C, Arquint C, Cornelis GR. 2011. Translocators YopB and YopD from Yersinia enterocolitica Form a Multimeric Integral Membrane Complex in Eukaryotic Cell Membranes. *J Bacteriol* **193**:6923–6928. doi:10.1128/JB.05555-11

Morrison C. 2015. Antibacterial antibodies gain traction. *Nat Rev Drug Discov* **14**:737–738. doi:10.1038/nrd4770

Mueller CA, Broz P, Cornelis GR. 2008. The type III secretion system tip complex and translocon. *Molecular Microbiology* **68**:1085–1095. doi:10.1111/j.1365-2958.2008.06237.x

Mulangu S, Dodd LE, Davey RT, Tshiani Mbaya O, Proschan M, Mukadi D, Lusakibanza Manzo M, Nzolo D, Tshomba Oloma A, Ibanda A, Ali R, Coulibaly S, Levine AC, Grais R, Diaz J, Lane HC, Muyembe-Tamfum J-J. 2019. A Randomized, Controlled Trial of Ebola Virus Disease Therapeutics. *N Engl J Med* **381**:2293–2303. doi:10.1056/NEJMoa1910993

Murray CJL, Ikuta KS, Sharara F, Swetschinski L, Robles Aguilar G, Gray A, Han C, Bisignano C, Rao P, Wool E, Johnson SC, Browne AJ, Chipeta MG, Fell F, Hackett S, Haines-Woodhouse G, Kashef Hamadani BH, Kumaran EAP, McManigal B, Achalapong S, Agarwal R, Akech S, Albertson S, Amuasi J, Andrews J, Aravkin A, Ashley E, Babin F-X, Bailey F, Baker S, Basnyat B, Bekker A, Bender R, Berkley JA, Bethou A, Bielicki J, Boonkasidecha S, Bukosia J, Carvalheiro C, Castañeda-Orjuela C, Chansamouth V, Chaurasia S, Chiurchiù S, Chowdhury F, Clotaire Donatien R, Cook AJ, Cooper B, Cressey TR, Criollo-Mora E, Cunningham M, Darboe S, Day NPJ, De Luca M, Dokova K, Dramowski A, Dunachie SJ, Duong Bich T, Eckmanns T, Eibach D, Emami A, Feasey N, Fisher-Pearson N, Forrest K, Garcia C, Garrett D, Gastmeier P, Giref AZ, Greer RC, Gupta V, Haller S, Haselbeck A, Hay SI, Holm M, Hopkins S, Hsia Y, Iregbu KC, Jacobs J, Jarovsky D, Javanmardi F, Jenney AWJ, Khorana M, Khusuwan S, Kissoon N, Kobeissi E, Kostyanev T, Krapp F, Krumkamp R, Kumar A, Kyu HH, Lim C, Lim K, Limmathurotsakul D, Loftus MJ, Lunn M, Ma J, Manoharan A, Marks F, May J, Mayxay M, Mturi N, Munera-Huertas T, Musicha P, Musila LA, Mussi-Pinhata MM, Naidu RN, Nakamura T, Nanavati R, Nangia S, Newton P, Ngoun C,

Novotney A, Nwakanma D, Obiero CW, Ochoa TJ, Olivas-Martinez A, Olliaro P, Ooko E, Ortiz-Brizuela E, Ounchanum P, Pak GD, Paredes JL, Peleg AY, Perrone C, Phe T, Phommasone K, Plakkal N, Ponce-de-Leon A, Raad M, Ramdin T, Rattanavong S, Riddell A, Roberts T, Robotham JV, Roca A, Rosenthal VD, Rudd KE, Russell N, Sader HS, Saengchan W, Schnall J, Scott JAG, Seekaew S, Sharland M, Shivamallappa M, Sifuentes-Osornio J, Simpson AJ, Steenkeste N, Stewardson AJ, Stoeva T, Tasak N, Thaiprakong A, Thwaites G, Tigoi C, Turner C, Turner P, Van Doorn HR, Velaphi S, Vongpradith A, Vongsouvath M, Vu H, Walsh T, Walson JL, Waner S, Wangrangsimakul T, Wannapinij P, Wozniak T, Young Sharma TEMW, Yu KC, Zheng P, Sartorius B, Lopez AD, Stergachis A, Moore C, Dolecek C, Naghavi M. 2022. Global burden of bacterial antimicrobial resistance in 2019: a systematic analysis. *The Lancet* **399**:629–655. doi:10.1016/S0140-6736(21)02724-0

Murshudov GN, Skubák P, Lebedev AA, Pannu NS, Steiner RA, Nicholls RA, Winn MD, Long F, Vagin AA. 2011. *REFMAC* 5 for the refinement of macromolecular crystal structures. *Acta Crystallogr D Biol Crystallogr* **67**:355–367. doi:10.1107/S0907444911001314

Nanao M, Ricard-Blum S, Di Guilmi A, Lemaire D, Lascoux D, Chabert J, Attree I, Dessen A. 2003. [No title found]. *BMC Microbiol* **3**:21. doi:10.1186/1471-2180-3-21

Ngo T-D, Plé S, Thomas A, Barette C, Fortuné A, Bouzidi Y, Fauvarque M-O, Pereira De Freitas R, Francisco Hilário F, Attrée I, Wong Y-S, Faudry E. 2019. Chimeric Protein–Protein Interface Inhibitors Allow Efficient Inhibition of Type III Secretion Machinery and *Pseudomonas aeruginosa* Virulence. *ACS Infect Dis* **5**:1843–1854. doi:10.1021/acsinfecdis.9b00154

Painter J, Merritt EA. 2006. *TLSMD* web server for the generation of multi-group TLS models. *J Appl Crystallogr* **39**:109–111. doi:10.1107/S0021889805038987

Pennini ME, De Marco A, Pelletier M, Bonnell J, Cvitkovic R, Beltramello M, Cameroni E, Bianchi S, Zatta F, Zhao W, Xiao X, Camara MM, DiGiandomenico A, Semenova E, Lanzavecchia A, Warrener P, Suzich J, Wang Q, Corti D, Stover CK. 2017. Immune stealth-driven O2 serotype prevalence and potential for therapeutic antibodies against multidrug resistant Klebsiella pneumoniae. *Nat Commun* **8**:1991. doi:10.1038/s41467-017-02223-7

Quinaud M, Chabert J, Faudry E, Neumann E, Lemaire D, Pastor A, Elsen S, Dessen A, Attree I. 2005. The PscE-PscF-PscG Complex Controls Type III Secretion Needle Biogenesis in Pseudomonas aeruginosa. *Journal of Biological Chemistry* **280**:36293–36300. doi:10.1074/jbc.M508089200

Quinaud M, Plé S, Job V, Contreras-Martel C, Simorre J-P, Attree I, Dessen A. 2007. Structure of the heterotrimeric complex that regulates type III secretion needle formation. *Proc Natl Acad Sci USA* **104**:7803–7808. doi:10.1073/pnas.0610098104

871 Rollenske T, Szijarto V, Lukasiewicz J, Guachalla LM, Stojkovic K, Hartl K, Stulik L,
872 Kocher S, Lasitschka F, Al-Saeedi M, Schröder-Braunstein J, Von Frankenberg M,
873 Gaebelein G, Hoffmann P, Klein S, Heeg K, Nagy E, Nagy G, Wardemann H. 2018.
874 Cross-specificity of protective human antibodies against Klebsiella pneumoniae LPS
875 O-antigen. *Nat Immunol* **19**:617–624. doi:10.1038/s41590-018-0106-2

876 Roy-Burman A, Savel RH, Racine S, Swanson BL, Revadigar NS, Fujimoto J, Sawa
877 T, Frank DW, Wiener-Kronish JP. 2001. Type III Protein Secretion Is Associated with
878 Death in Lower Respiratory and Systemic *Pseudomonas aeruginosa* Infections. *J*
879 *INFECT DIS* **183**:1767–1774. doi:10.1086/320737

880 Sawa, Kinoshita, Inoue, Ohara, Moriyama. 2019. Immunoglobulin for Treating
881 Bacterial Infections: One More Mechanism of Action. *Antibodies* **8**:52.
882 doi:10.3390/antib8040052
883

884 Schoehn G, Di Guilmi AM, Lemaire D, Attree I, Weissenhorn W, Dessen A. 2003.
885 Oligomerization of type III secretion proteins PopB and PopD precedes pore formation
886 in Pseudomonas. *EMBO J*. **22**(19):4957-67. doi:10.1093/emboj/cdg499.

887 Serapio-Palacios A, Finlay BB. 2020. Dynamics of expression, secretion and
888 translocation of type III effectors during enteropathogenic Escherichia coli infection.
889 *Current Opinion in Microbiology* **54**:67–76. doi:10.1016/j.mib.2019.12.001

890 Simonis A, Kreer C, Albus A, Rox K, Yuan B, Holzmann D, Wilms JA, Zuber S, Kottege
891 L, Winter S, Meyer M, Schmitt K, Gruell H, Theobald SJ, Hellmann A-M, Meyer C,
892 Ercanoglu MS, Cramer N, Munder A, Hallek M, Fätkenheuer G, Koch M, Seifert H,
893 Rietschel E, Marlovits TC, Van Koningsbruggen-Rietschel S, Klein F, Rybniker J. 2023.
894 Discovery of highly neutralizing human antibodies targeting Pseudomonas aeruginosa.
895 *Cell* **186**:5098-5113.e19. doi:10.1016/j.cell.2023.10.002

896 Tabor DE, Oganesyan V, Keller AE, Yu L, McLaughlin RE, Song E, Warrener P,
897 Rosenthal K, Esser M, Qi Y, Ruzin A, Stover CK, DiGiandomenico A. 2018.
898 Pseudomonas aeruginosa PcrV and Psl, the Molecular Targets of Bispecific Antibody
899 MEDI3902, Are Conserved Among Diverse Global Clinical Isolates. *The Journal of*
900 *Infectious Diseases*. doi:10.1093/infdis/jiy438

901 Tickle IJ. 2007. Experimental determination of optimal root-mean-square deviations of
902 macromolecular bond lengths and angles from their restrained ideal values. *Acta*
903 *Crystallogr D Biol Crystallogr* **63**:1274–1281. doi:10.1107/S0907444907050196

904 Vacca F, Sala C, Rappuoli R. 2022. Monoclonal Antibodies for Bacterial Pathogens:
905 Mechanisms of Action and Engineering Approaches for Enhanced Effector Functions.
906 *Biomedicines* **10**:2126. doi:10.3390/biomedicines10092126

907 Verove J, Bernarde C, Bohn Y-ST, Boulay F, Rabiet M-J, Attree I, Cretin F. 2012.
908 Injection of Pseudomonas aeruginosa Exo Toxins into Host Cells Can Be Modulated
909 by Host Factors at the Level of Translocon Assembly and/or Activity. *PLoS ONE*
910 **7**:e30488. doi:10.1371/journal.pone.0030488

911 Watson A, Li H, Ma B, Weiss R, Bendayan D, Abramovitz L, Ben-Shalom N, Mor M,
912 Pinko E, Bar Oz M, Wang Z, Du F, Lu Y, Rybniker J, Dahan R, Huang H, Barkan D,
913 Xiang Y, Javid B, Freund NT. 2021. Human antibodies targeting a Mycobacterium
914 transporter protein mediate protection against tuberculosis. *Nat Commun* **12**:602.
915 doi:10.1038/s41467-021-20930-0

916 West SEH, Schweizer HP, Dall C, Sample AK, Runyen-Janecky LJ. 1994.
917 Construction of improved Escherichia-Pseudomonas shuttle vectors derived from
918 pUC18/19 and sequence of the region required for their replication in Pseudomonas
919 aeruginosa. *Gene* **148**:81–86. doi:10.1016/0378-1119(94)90237-2

920 Yaeger LN, Coles VE, Chan DCK, Burrows LL. 2021. How to kill *Pseudomonas* —
921 emerging therapies for a challenging pathogen. *Annals of the New York Academy of*
922 *Sciences* **1496**:59–81. doi:10.1111/nyas.14596

923 Zucker F, Champ PC, Merritt EA. 2010. Validation of crystallographic models
924 containing TLS or other descriptions of anisotropy. *Acta Crystallogr D Biol Crystallogr*
925 **66**:889–900. doi:10.1107/S0907444910020421

926
927

928 **FIGURES**

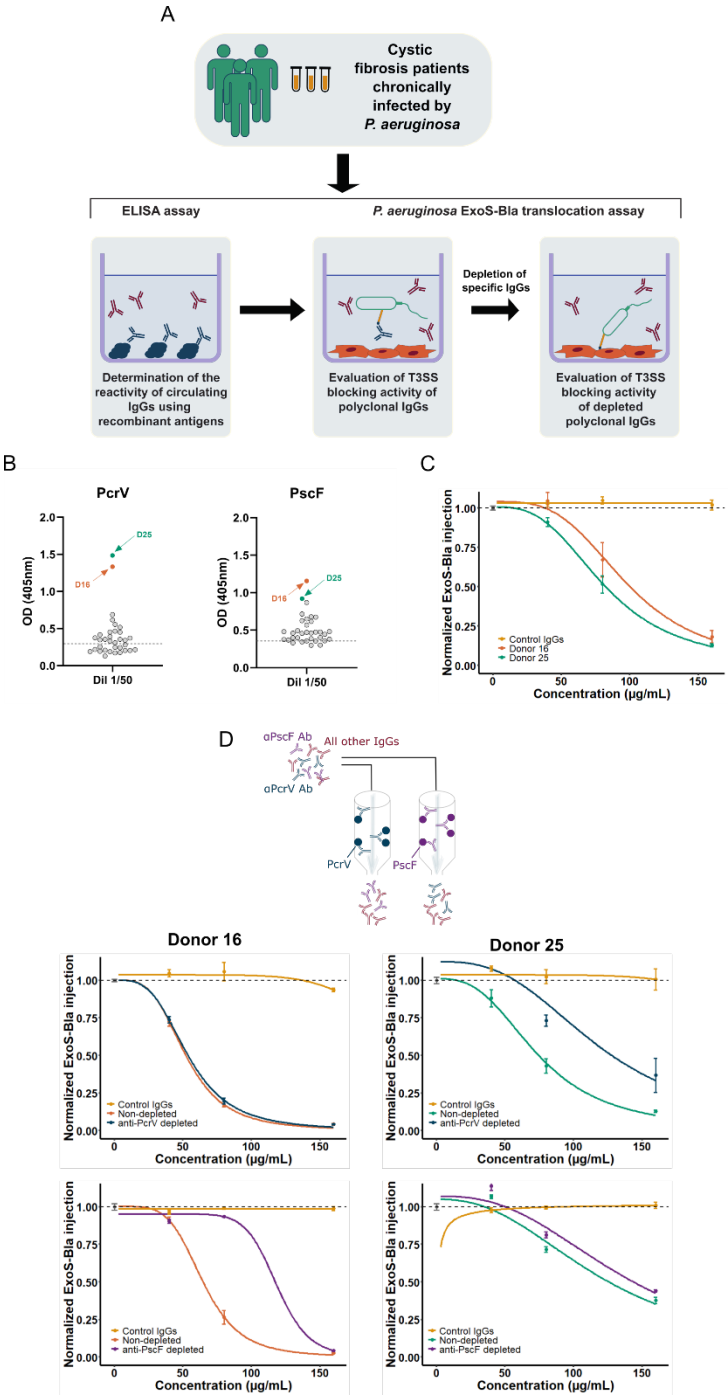

929

930 **Figure 1. Screening workflow and donor selection**

931 (A) Schematic representation of the workflow from patient selection to evaluation of
932 T3SS-blocking activity. (B) ELISA results indicating that sera of donors 16 and 25
933 possess the highest Ab titers against recombinant PcrV and PscF. (C) ExoS-Bla
934 translocation blocking activity of serum from donors 16 and 25. (D) (top) scheme of
935 depletion experiment of specific Abs on either PscF- or PcrV–loaded columns. (bottom)
936 blocking activity of depleted sera for both donors.

A

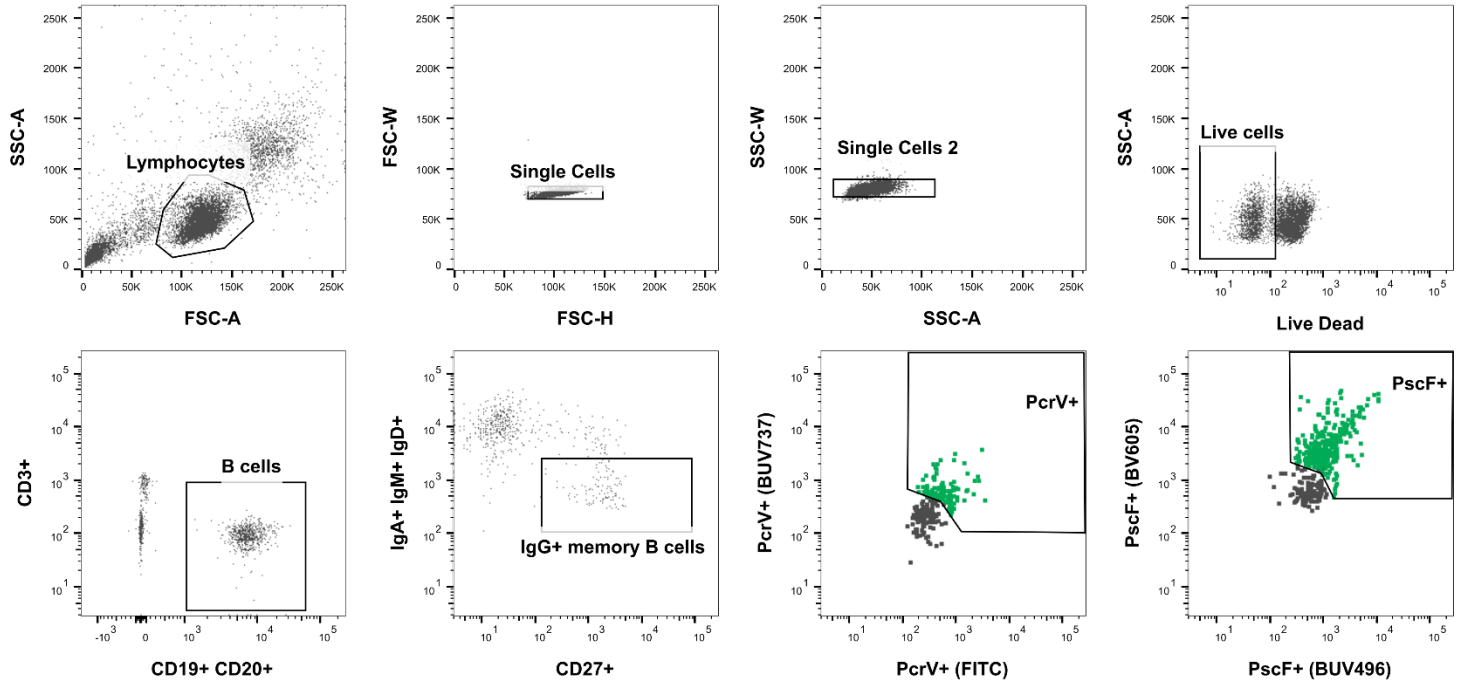

B

Anti-PcrV mAbs	EC_{50} (µg/mL)	ExoS-Bla inhibition
P3D6	0.03	24 %
P5B3	0.04	94 %
P3G9	0.08	No inhibition
P5E10	0.17	No inhibition
Anti-PscF mAbs	EC_{50} (µg/mL)	ExoS-Bla inhibition
P5G10	0.01	No inhibition
P1B7	0.07	No inhibition
P5D5	0.07	No inhibition
P1D5	0.18	No inhibition
P1B4	0.24	No inhibition
P3G6	1.28	No inhibition
P3G2	2.08	No inhibition
P1F5	4.65	No inhibition
P3G7	10.61	No inhibition
P1D7	>30	No inhibition

Figure 2. Selection of B cells from donors 16 and 25. (A) B cells sorting and isolation using PscF and PcrV baits. (B) Table summarizing the EC_{50} values of selected Abs obtained by ELISA and the percentage of inhibition of ExoS-Bla injection into epithelial cells at 100 µg/mL.

A

Variant	Amino acid positions			
	6	9	21	225
V1 (PAO1-like)	Leu	Ala	Ser	Ser
V2 (CHA-like)	Leu	Ala	Ser	Arg
V3 (PA14-like)	Phe	Ala	Pro	Lys
V4 (PA103-like)	Phe	Gly	Pro	Arg
V5	Phe	Gly	Pro	Lys

B

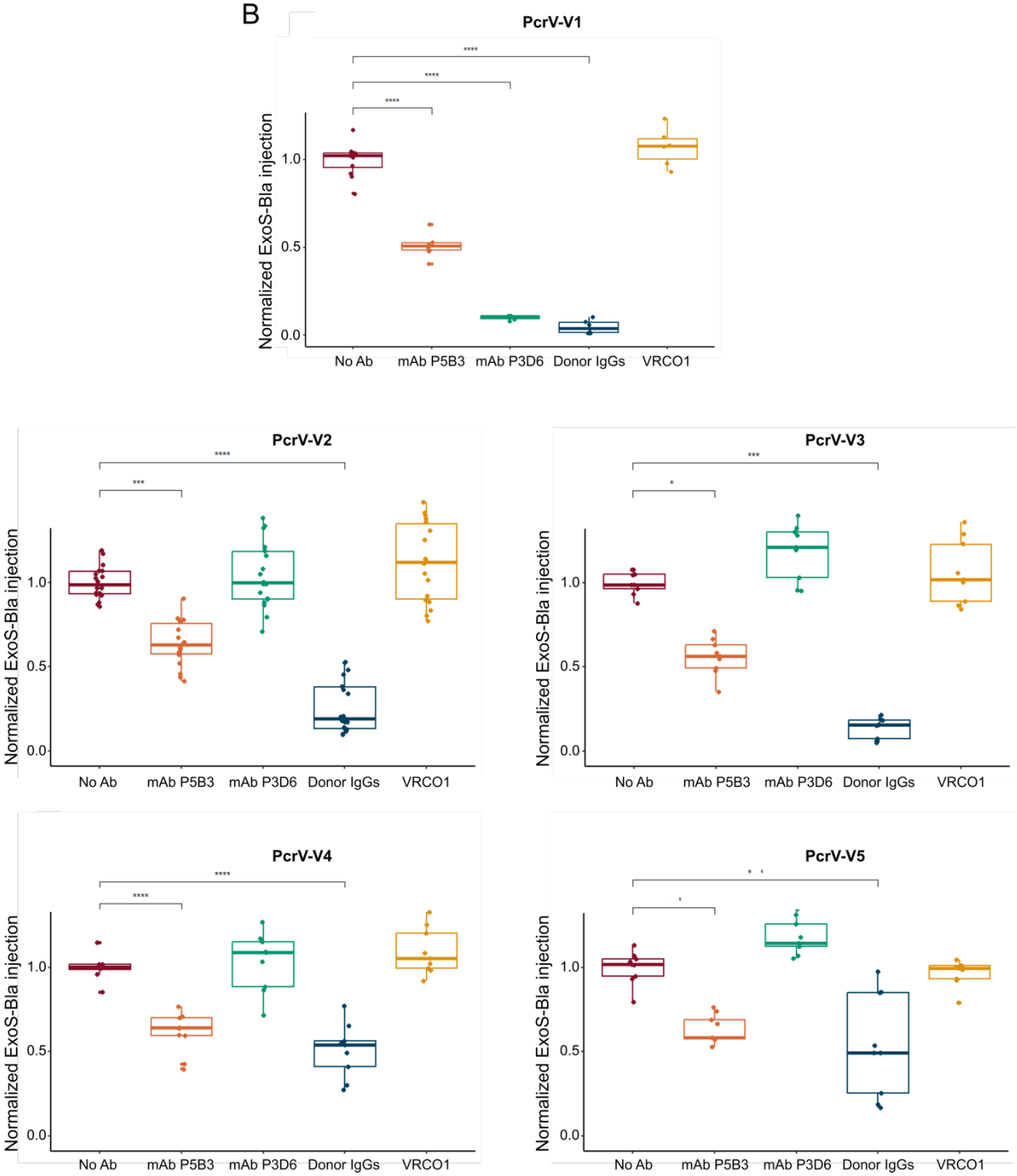

945 **Figure 3**. **mAbs P5B3 and P3D6 activity on PcrV variants**. (A) PcrV variability in
946 clinical strains. The most variable position (225) can either be Ser, Arg or Lys.
947 Representative strains are indicated when available (PAO1 for V1, CHA for V2, PA14
948 for V3 and PA103 for V4). (B) Inhibition of ExoS-Bla activity following infection of A549
949 epithelial cells with *P. aeruginosa* expressing the V1 variant. IgGs from donor 25, as
950 well as mAbs P5B3 and P3D6 block ExoS-Bla injection, while the control mAb VRCO1
951 is inefficient. While P3D6 displays significant inhibition only towards V1, P5B3 displays
952 dose-dependent inhibition on all five variants (see also Supplementary Figure 1).

953

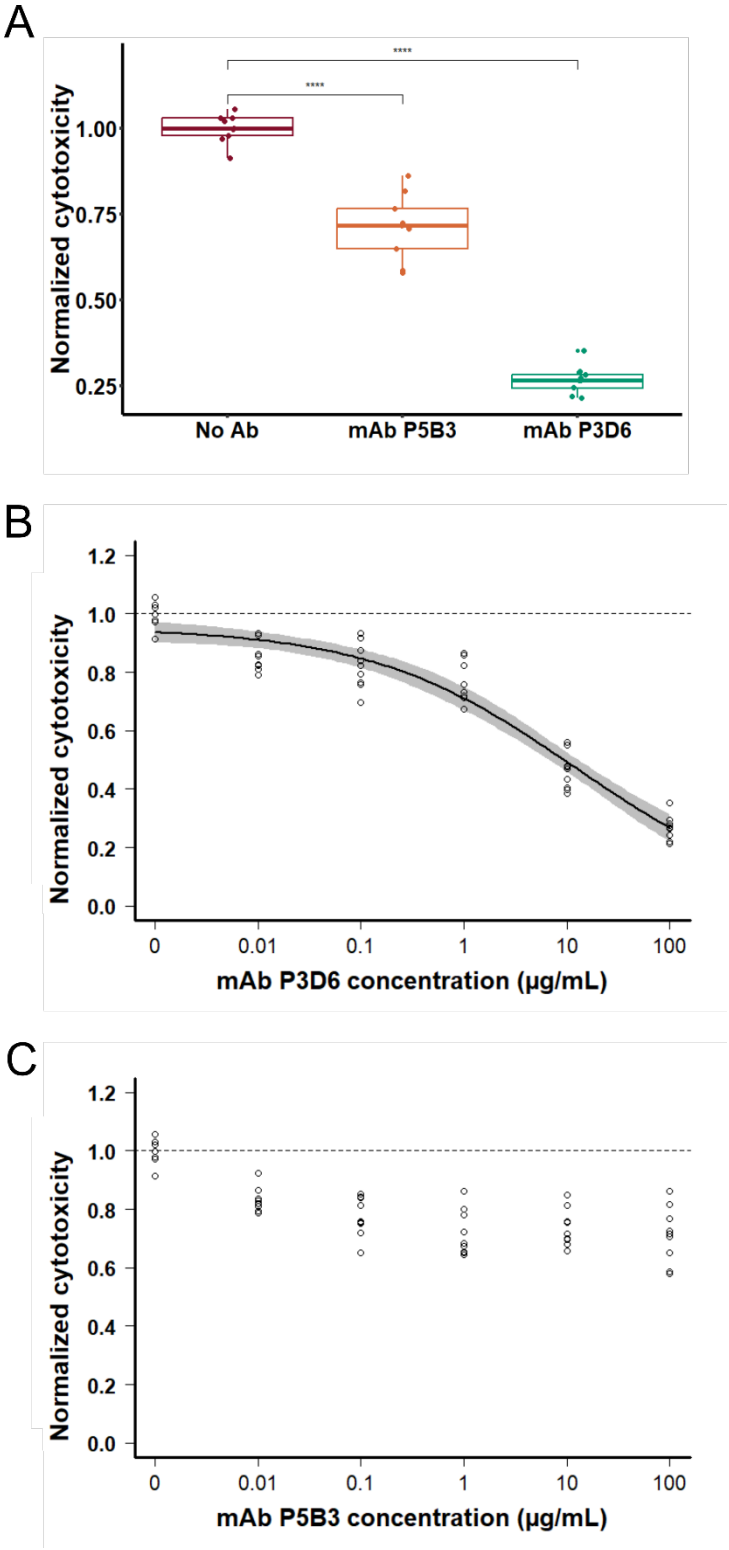

Figure 4. mAb P3D6 efficiently inhibits the PopB/PopD translocation pore. J774 macrophages were infected with *P. aeruginosa* strain (PAO1, V1) deprived of all three T3SS toxins. The cell death (cytotoxicity) resulting from insertion of the translocon pore was measured by propidium iodide incorporation and normalized to the wild-type strain without addition of mAbs. (A) Both P3D6 and P5B3 mAbs significantly reduce pore formation at 100 µg/mL. (B, C) Only P3D6 exhibits a significant dose-response inhibitory effect on cytotoxicity towards J774 cells with an IC_{50} of 11.8 µg/mL.

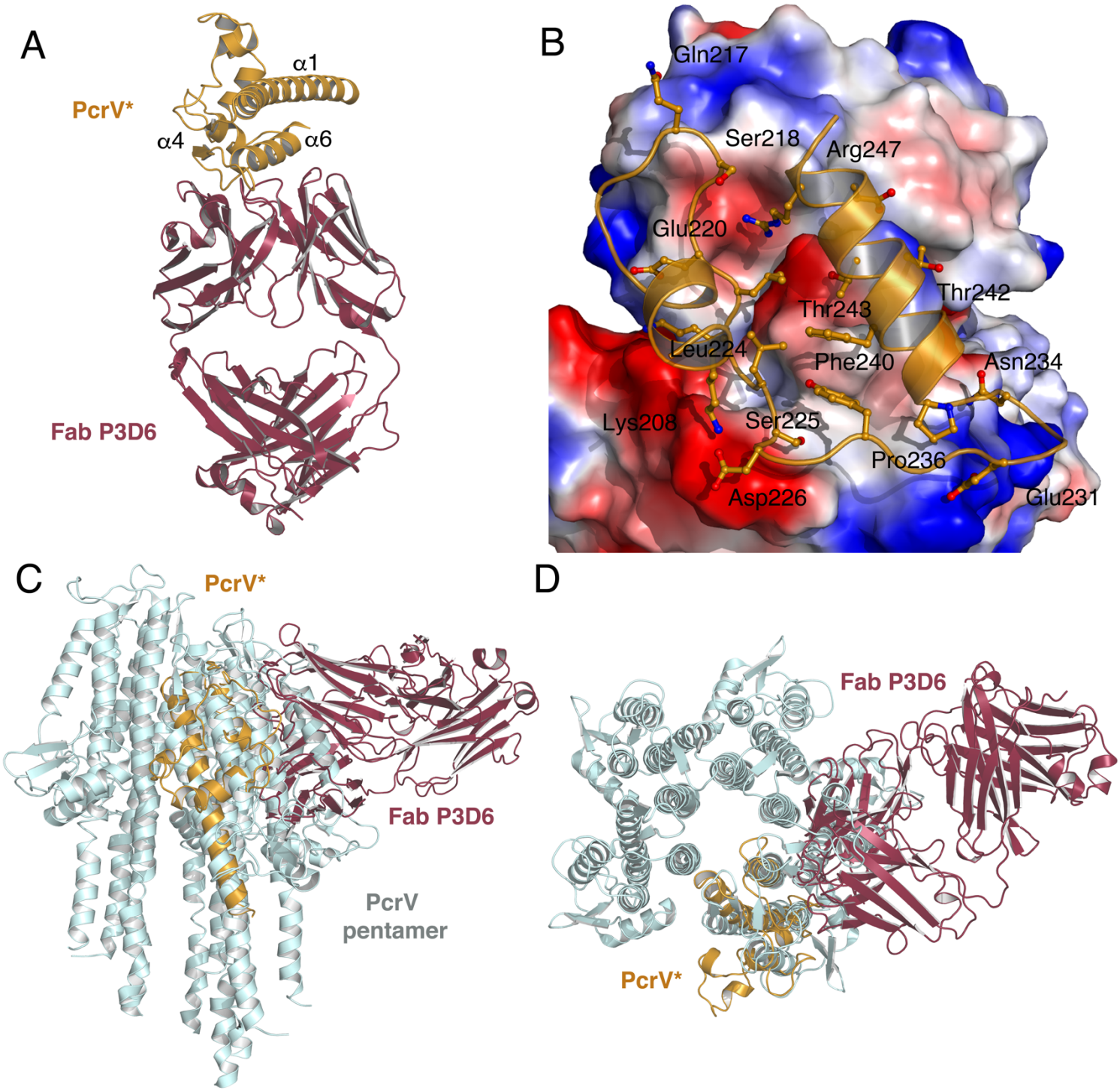

Figure 5. Structure of Fab P3D6 in complex with PcrV*. (A) Crystal structure of Fab P3D6 in complex with PcrV*. Fab P3D6 is shown in brown, while PcrV* is in orange. Contacts are made between PcrV* and an interaction platform formed by both HC and LC of P3D6. (B) Closeup of the interaction between PcrV* and P3D6, with the latter being shown as an electrostatic surface where acidic regions are shown in red, and basic in blue. Side (C) and top (D) views of the modeled PcrV pentamer, in light blue) onto which the structure shown in (A) was overlaid. Note that the bound Fab clashes with a neighboring PcrV protomer, precluding the formation of the pentamer.

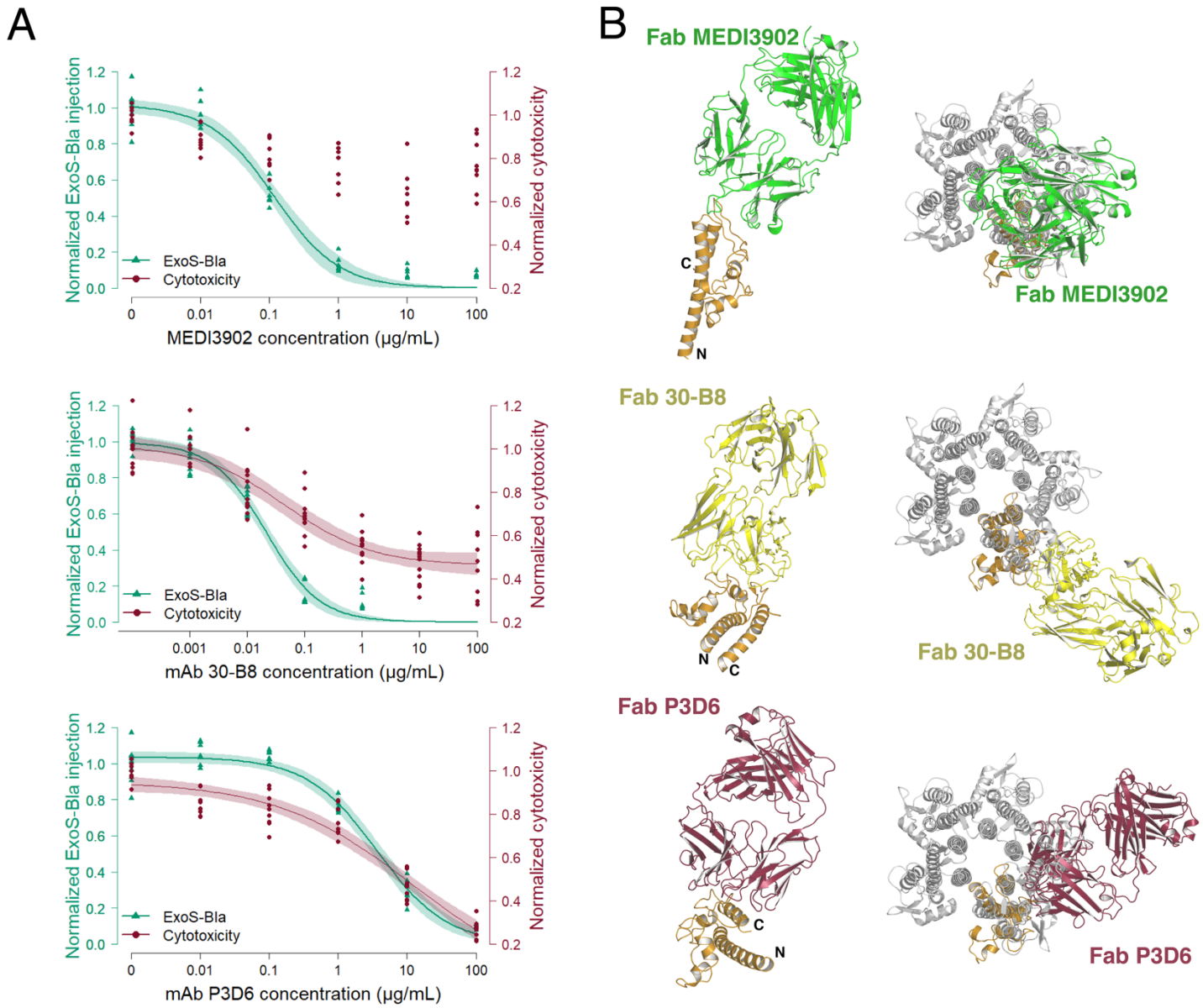

Figure 6. Functional and structural comparisons between anti-PcrV mAbs.

(A) Dose-dependent inhibition of T3SS in two functional assays reflecting toxin injection (ExoS-Bla injection) and translocon assembly (normalized J774 macrophage cytotoxicity) for three mAbs.

(B) Structures of PcrV-Fab complexes in the context of a PcrV monomer, as well as of a pentamer modeled based on the cryo-EM structure of SipD (Guo and Galan 2021). Fab P3D6 binds to a PcrV monomer but clashes with adjacent protomers in the context of the pentamer, while Fab MEDI3902 clashes with other Fab molecules. Fab 30-B8 binds to both the PcrV monomer and all pentamer protomers without clashes. N- and C- termini of PcrV are indicated in all structures, which are referenced in the main text.

AUTHOR CONTRIBUTIONS

JMD, EF, CCM, FC, LSDD, AA, IB, VTC and FC performed experiments and analyzed the data; EF, CCM and LSDD prepared the figures; DF and YC provided the tools and materials; IA, AD and PP designed the study, analyzed the data, and wrote the manuscript. All authors participated in discussions and editing of the final version of the manuscript.

DECLARATION OF INTERESTS

The authors declare no competing interests.